Supplement of

Improving snow albedo modeling in E3SM land model (version 2.0) and assessing its impacts on snow and surface fluxes over the Tibetan Plateau

Dalei Hao[1], Gautam Bisht[1], Cenlin He[2], Edward Bair[3], Huilin Huang[1], Cheng Dang[4], Karl Rittger[5], Yu Gu[6], Hailong Wang[1], Yun Qian[1] and L. Ruby Leung[1]

[1]Atmospheric Sciences and Global Change Division, Pacific Northwest National Laboratory, Richland, WA, USA
[2]Research Applications Laboratory, National Center for Atmospheric Research, Boulder, CO, USA
[3]Earth Research Institute, University of California, Santa Barbara, CA, USA
[4]Joint Center for Satellite Data Assimilation, University Corporation for Atmospheric Research, Boulder, CO, USA
[5]Institute for Arctic and Alpine Research, University of Colorado, Boulder, CO, USA
[6]Joint Institute for Regional Earth System Science and Engineering and Department of Atmospheric and Oceanic Sciences, University of California, Los Angeles, CA, USA

Correspondence to: Dalei Hao (dalei.hao@pnnl.gov)

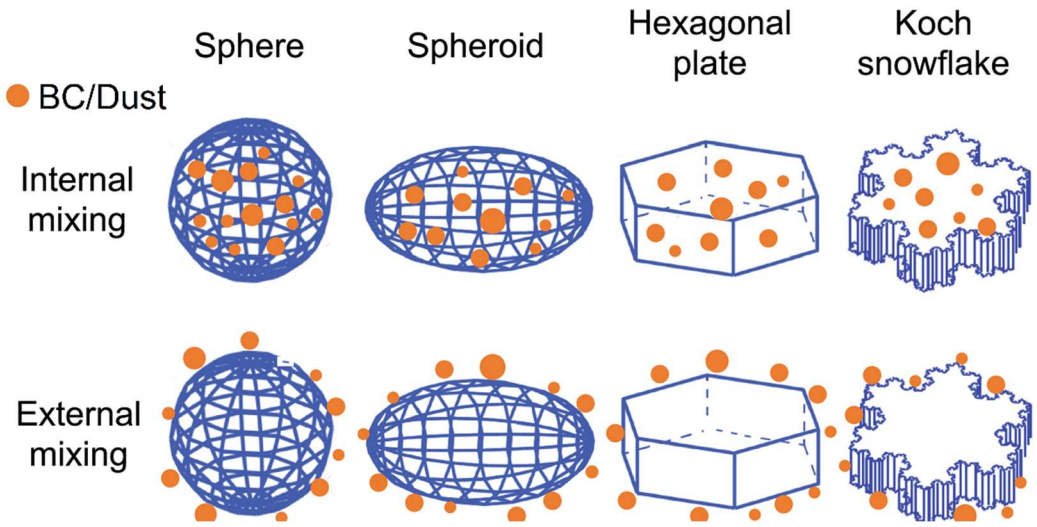

Figure S1: Schematics of four typical snow grain shapes: sphere, spheroid, hexagonal plate and Koch snowflake, and two different mixing states of BC-snow or dust-snow: internal and external. This figure is adapted from (He et al., 2019).

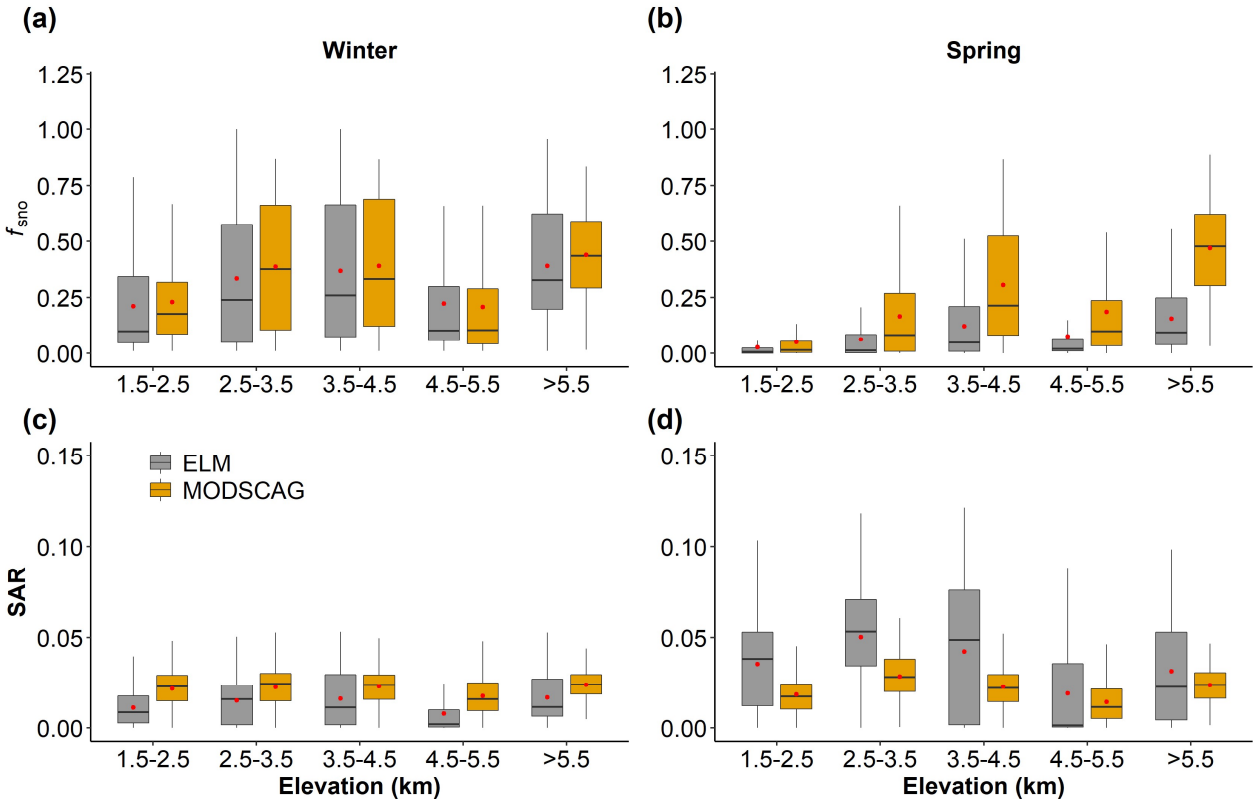

Figure S2: Statistical distributions of (a,b) f_{sno} and (c,d) SAR induced by LAPs for winter and spring in the co-located areas of ELM and MODSCAG.

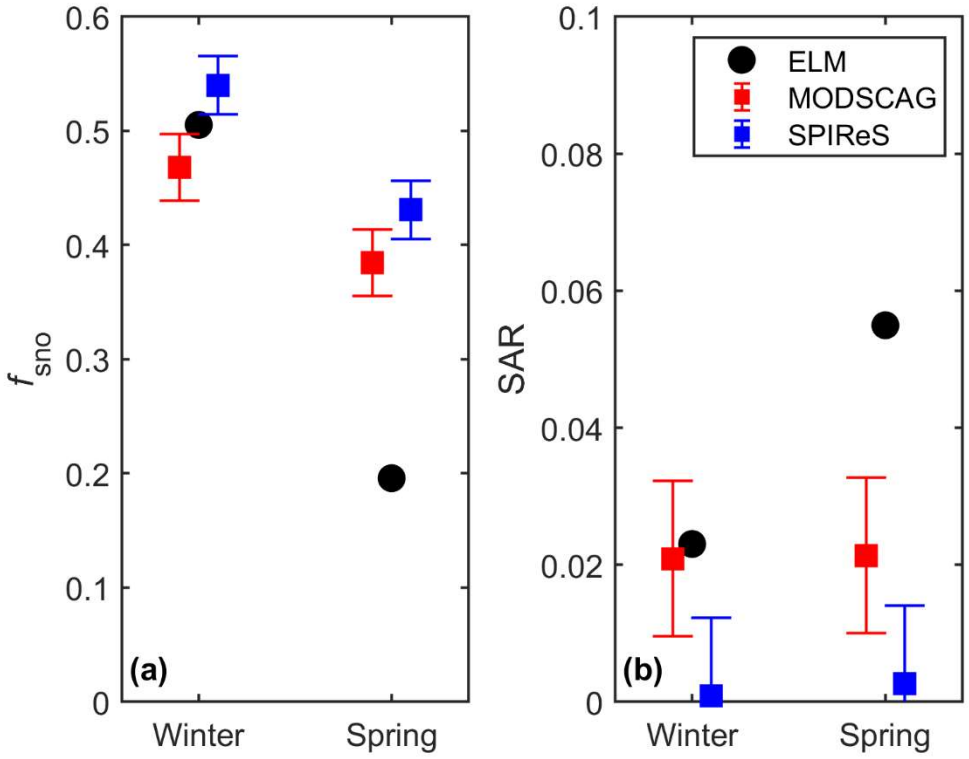

Figure S3. The area-weighted average (a) f_{sno} and (b) SAR induced by LAPs for winter and spring in the overlapping areas (enclosed by the red lines in Figure 2) of ELM, MODSCAG and SPIReS.. The bar width represents the uncertainty bounds of MODSCAG and SPIReS from (Bair et al., 2021).

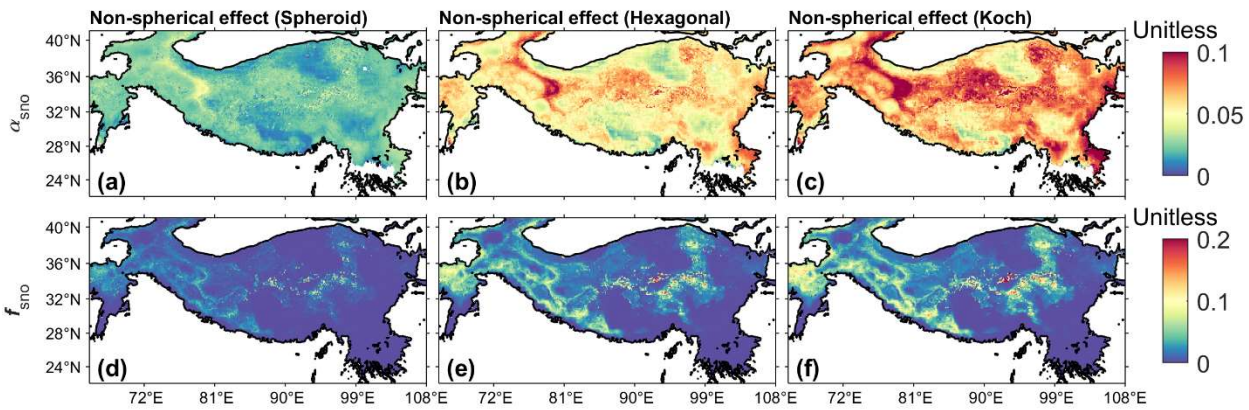

Figure S4: The differences in (a-c) A_{sno} and (d-f) f_{sno} between different snow grain shapes. (a,d) Difference between spheroid and sphere, (b,e) difference between hexagonal plate and sphere and (c,f) difference between Koch snowflake and sphere for winter. The specific calculation methods are listed in Table 2.

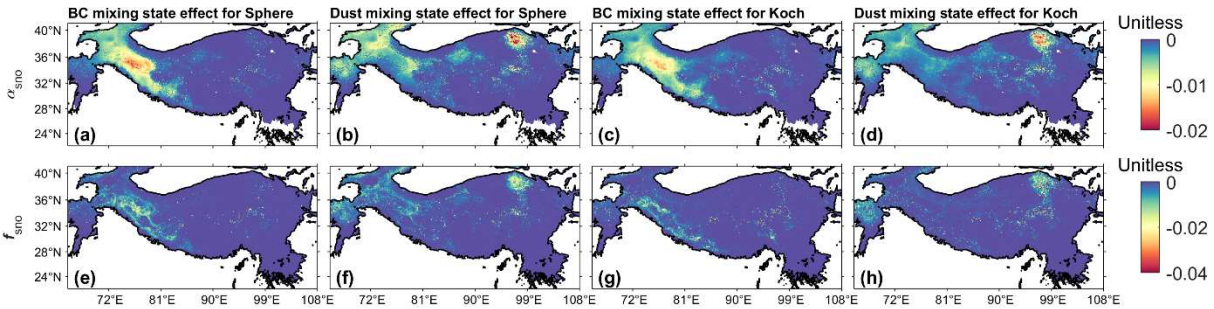

Figure S5: The differences in (a-d) A_{sno} and (e-h) f_{sno} between different mixing states (internal - external) of snow-LAP: (a,e) BC for sphere snow grain shape, (b,f) dust for sphere snow grain shape, (c,g) BC for Koch snowflake grain shape, and (d,h) dust for Koch snowflake grain shape for winter. The specific calculation methods are listed in Table 2.

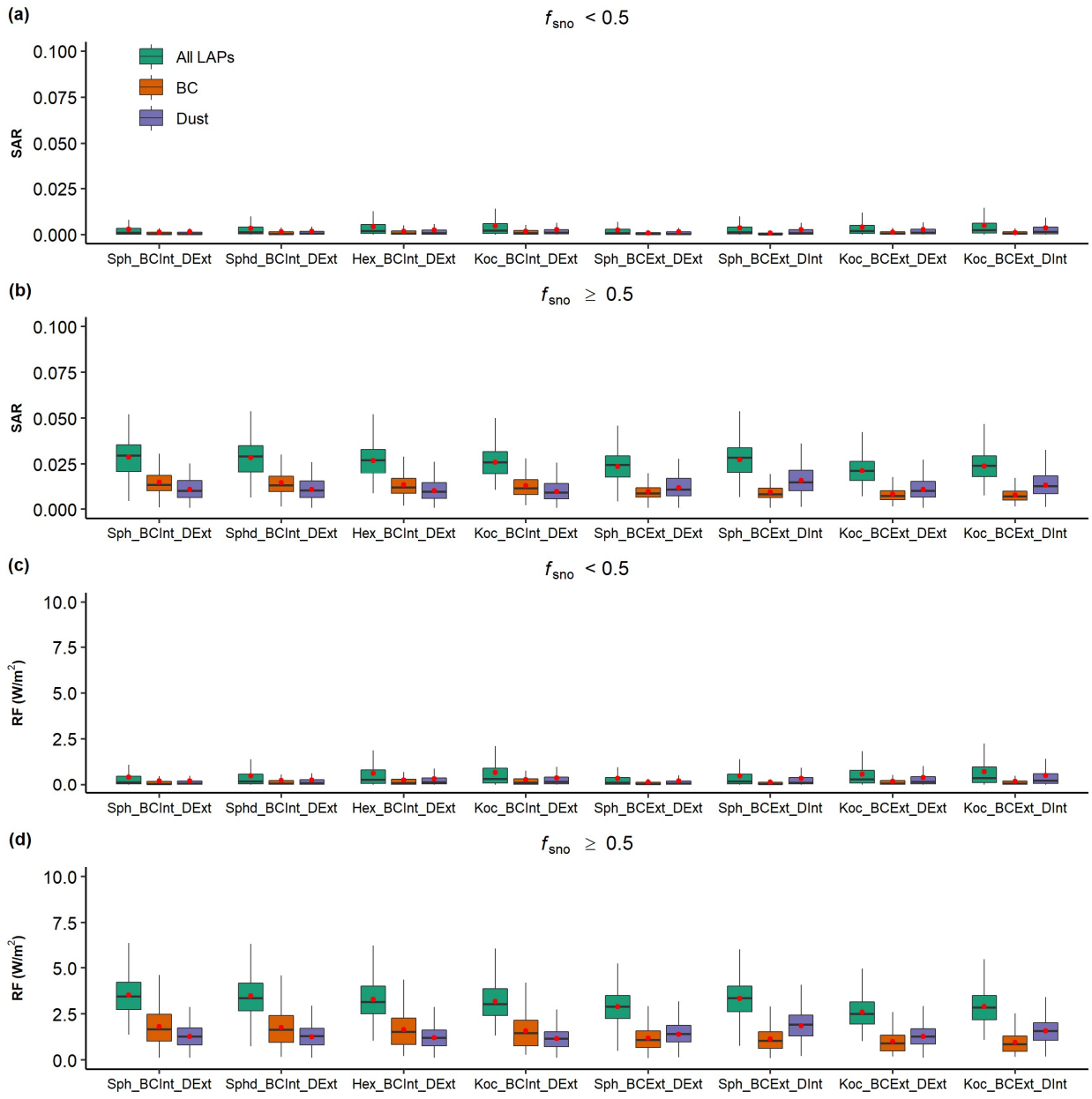

Figure S6: Boxplots of (a,b) SAR and (c,d) RF from all LAPs, BC and dust for different snow cover fractions: (a,c) f_{sno}<0.5 and (b,d) f_{sno}≥0.5 in winter under different cases listed in Table 1. For the case ID labelled in x-axis, the '_PP' suffix is omitted to keep them simplified. Red circles represent the mean values.

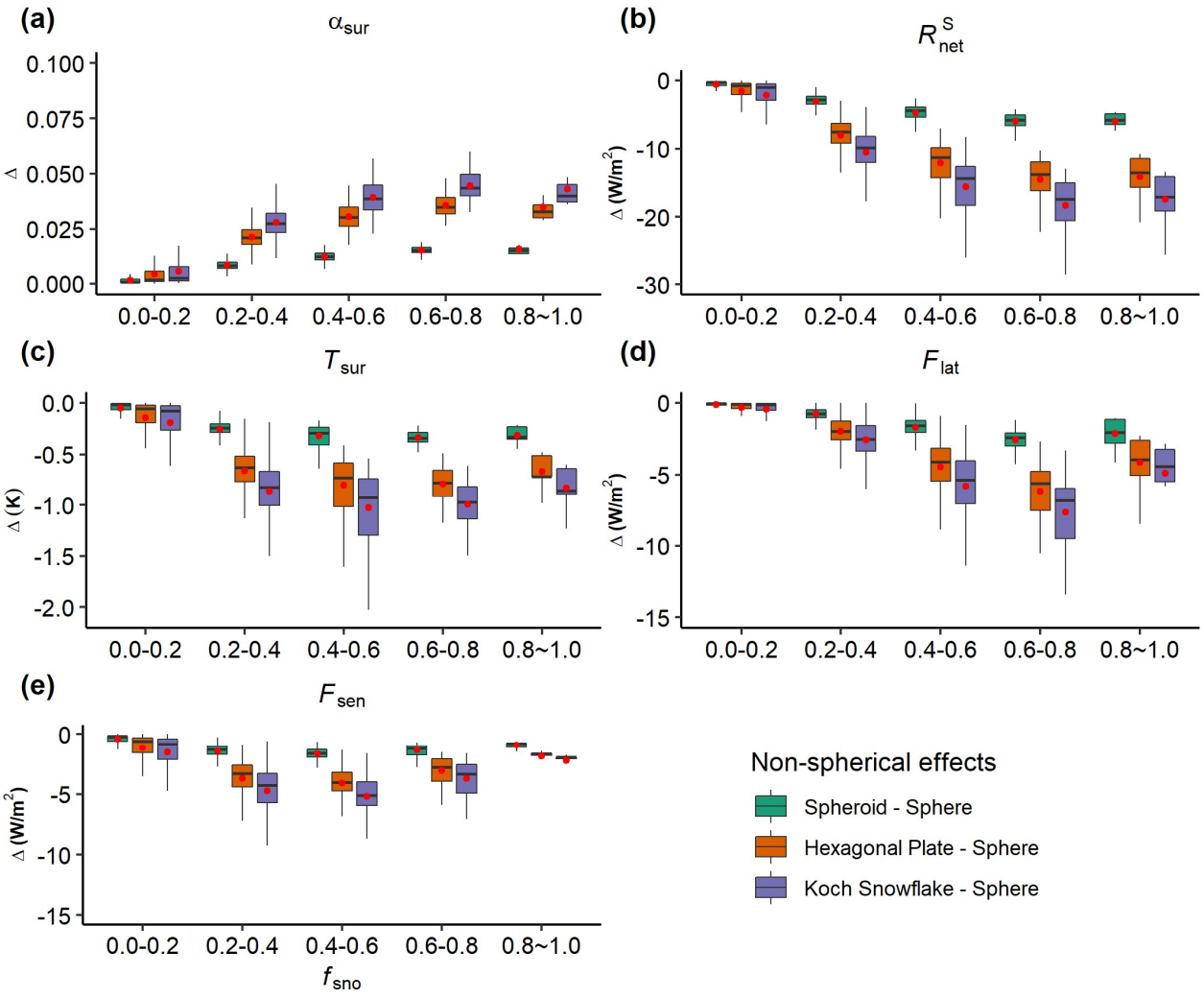

Figure S7: The boxplots of the differences (Δ) in surface energy cycle terms: (a) surface albedo (α_{sur}), (b) net solar radiation (R^{s}_{net}), (c) surface temperature (T_{sur}), (d) latent heat flux (F_{lat}) and (e) sensible heat flux (F_{sen}), between different snow grain shapes: spheroid – sphere, hexagonal plate – sphere and Koch snowflake – sphere under different snow cover fractions (f_{sno}) for spring. See Table 2 for the specific calculation methods.

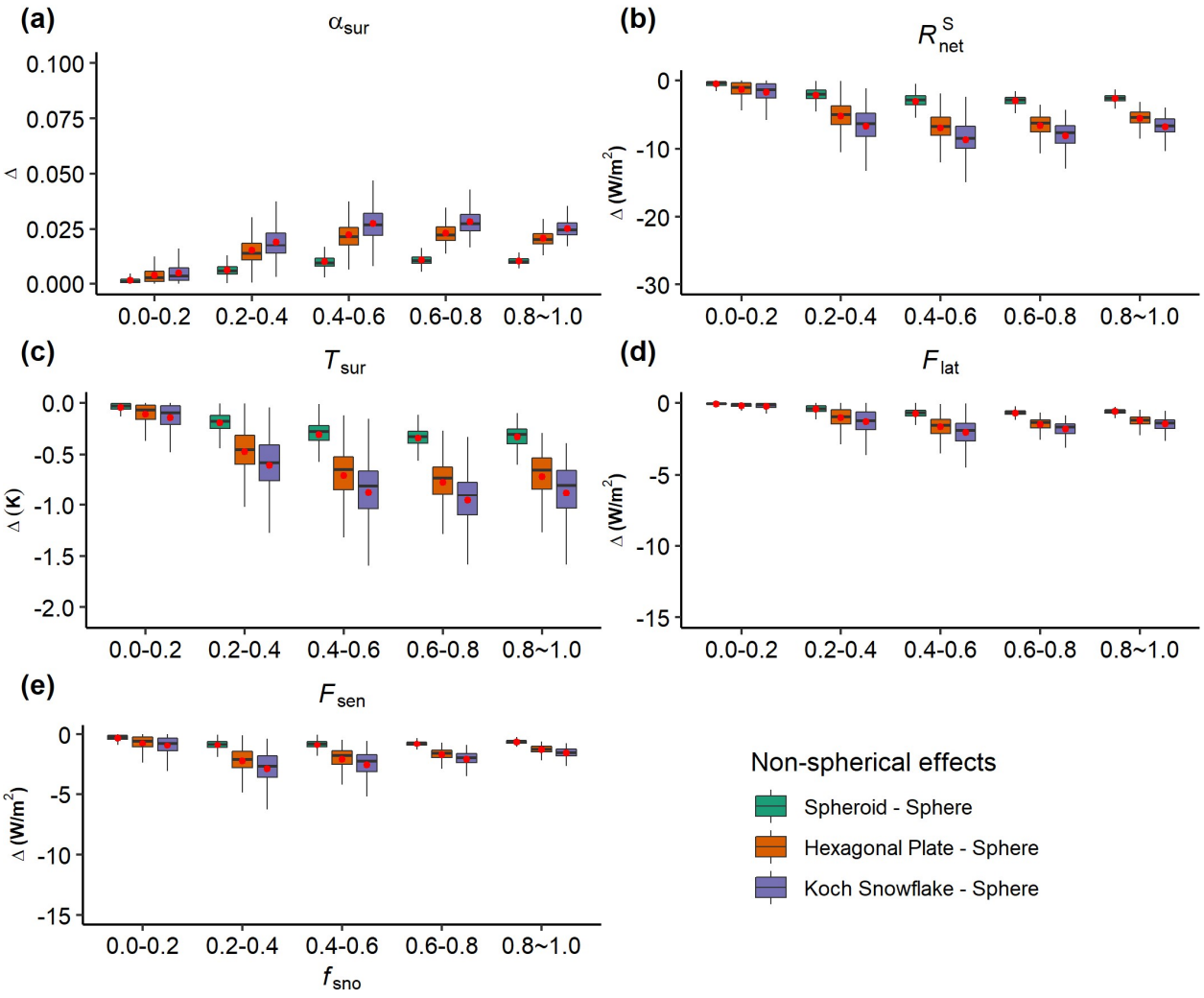

Figure S8: Same as Figure S7 except for winter.

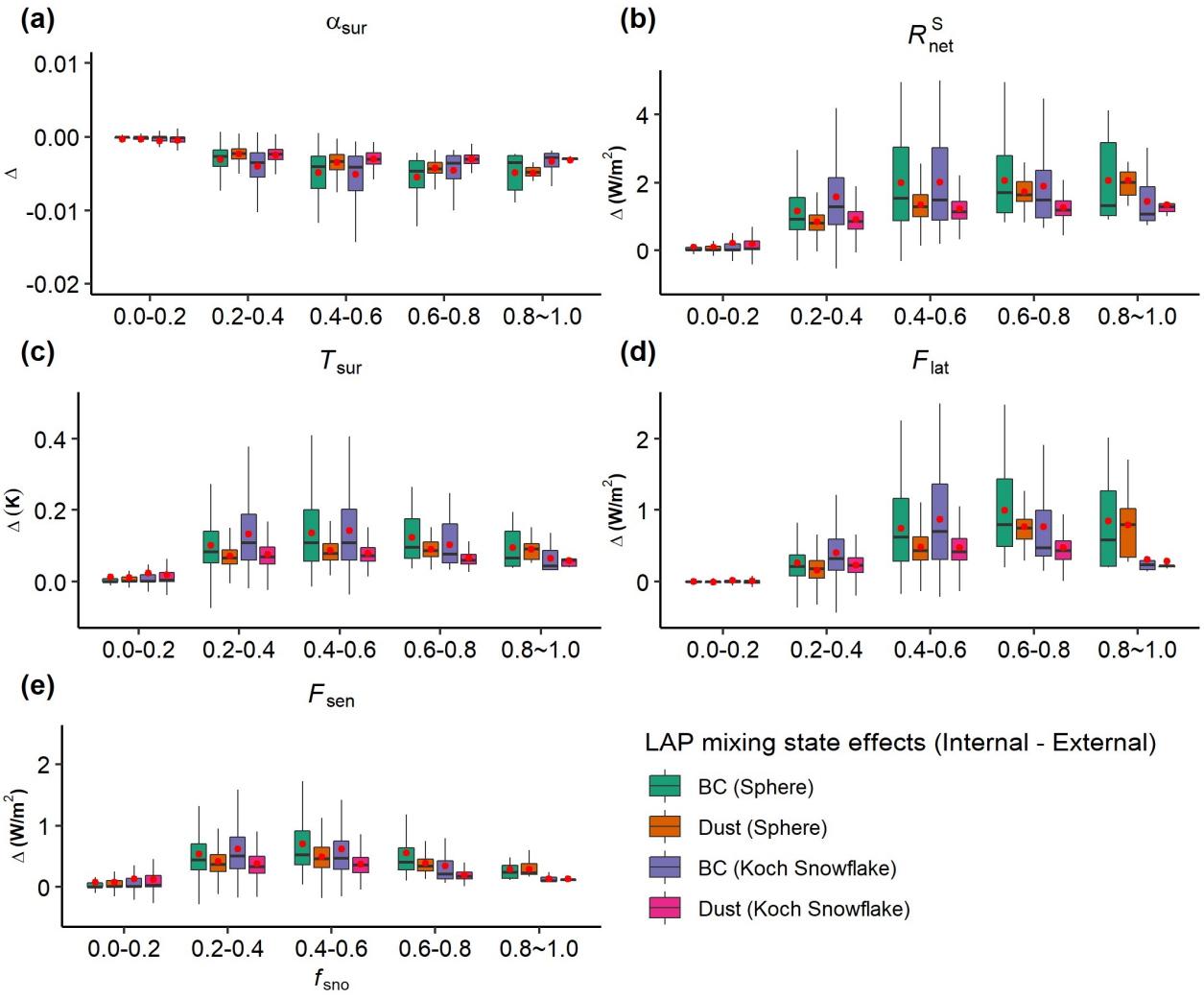

Figure S9: The boxplots of the differences (Δ) in surface energy terms: (a) surface albedo (α_{sur}), (b) net solar radiation ($\boldsymbol{R^{s}_{net}}$), (c) surface temperature (T_{sur}), (d) latent heat flux (F_{lat}) and (e) sensible heat flux (F_{sen}), between different mixing states (internal - external) of snow-LAP: BC(sphere), dust(sphere), BC(Koch snowflake) and dust(Koch snowflake) under different snow cover fractions for spring. See Table 2 for the specific calculation methods.

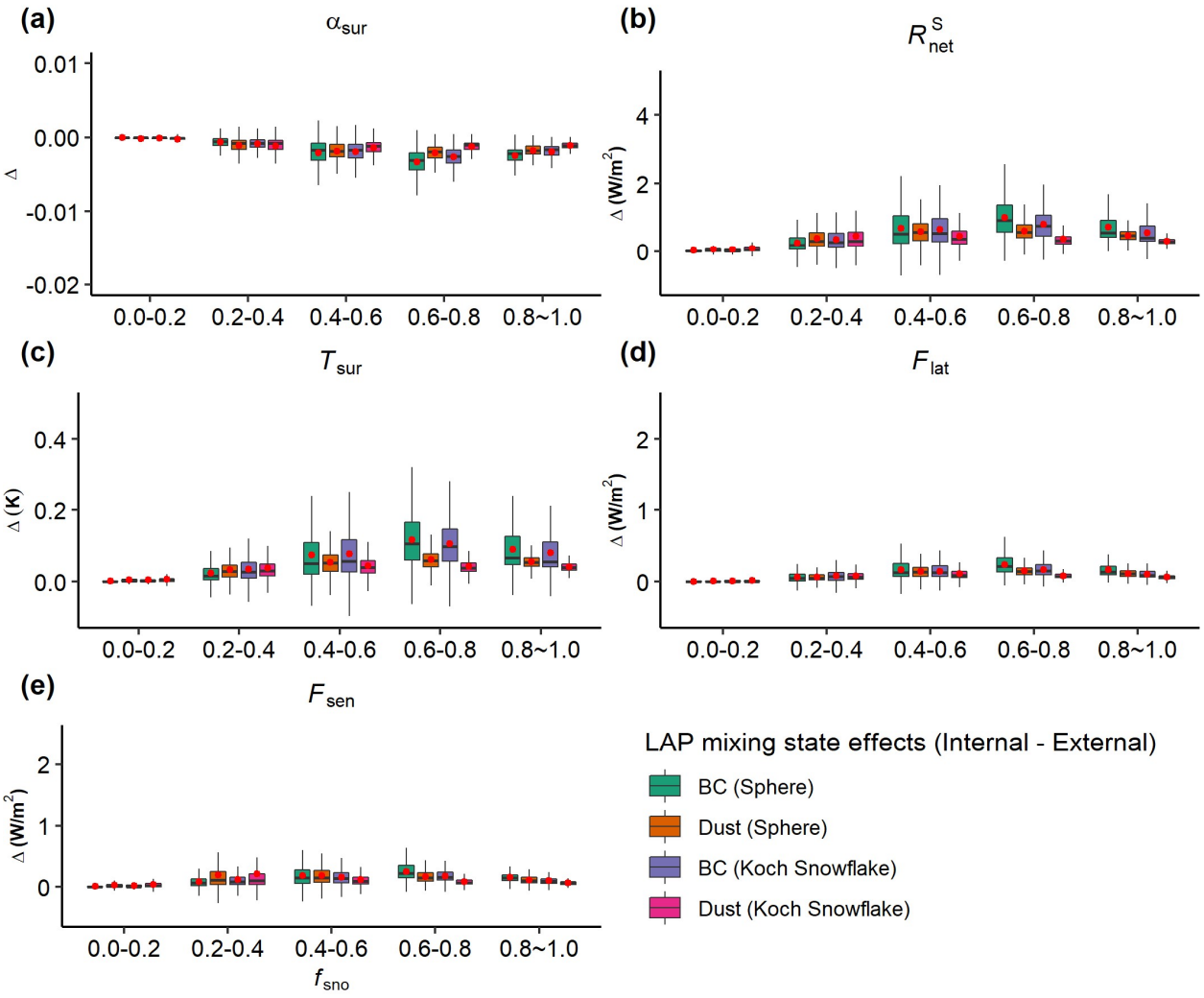

Figure S10: Same as Figure S9 except for winter.

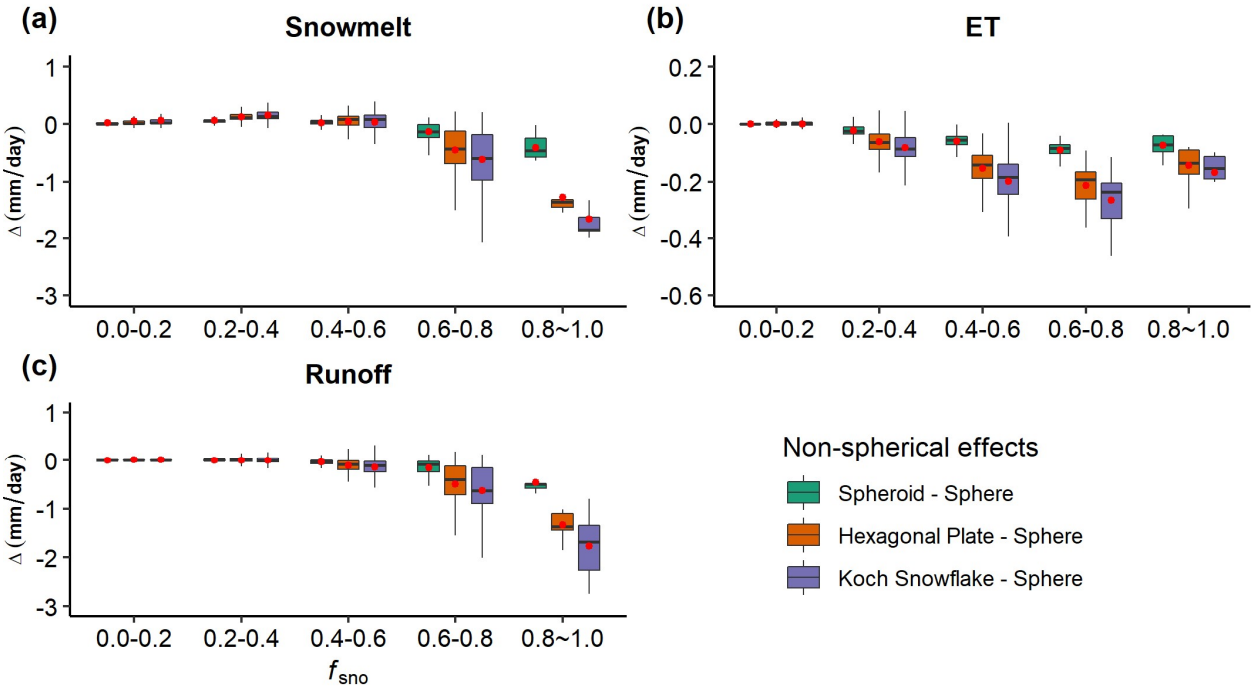

Figure S11: Same as Figure S7, except for hydrological terms: (a) snowmelt, (b) ET, and (c) runoff.

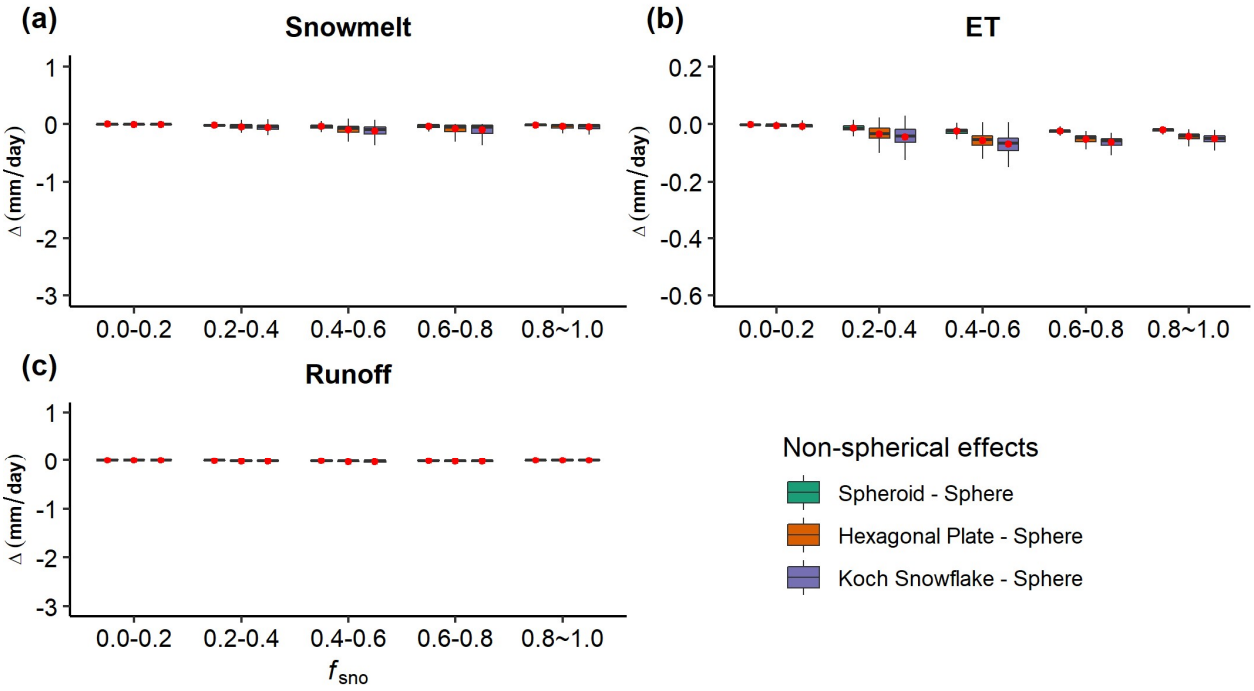

Figure S12: Same as Figure S8, except for hydrological terms: (a) snowmelt, (b) ET, and (c) runoff.

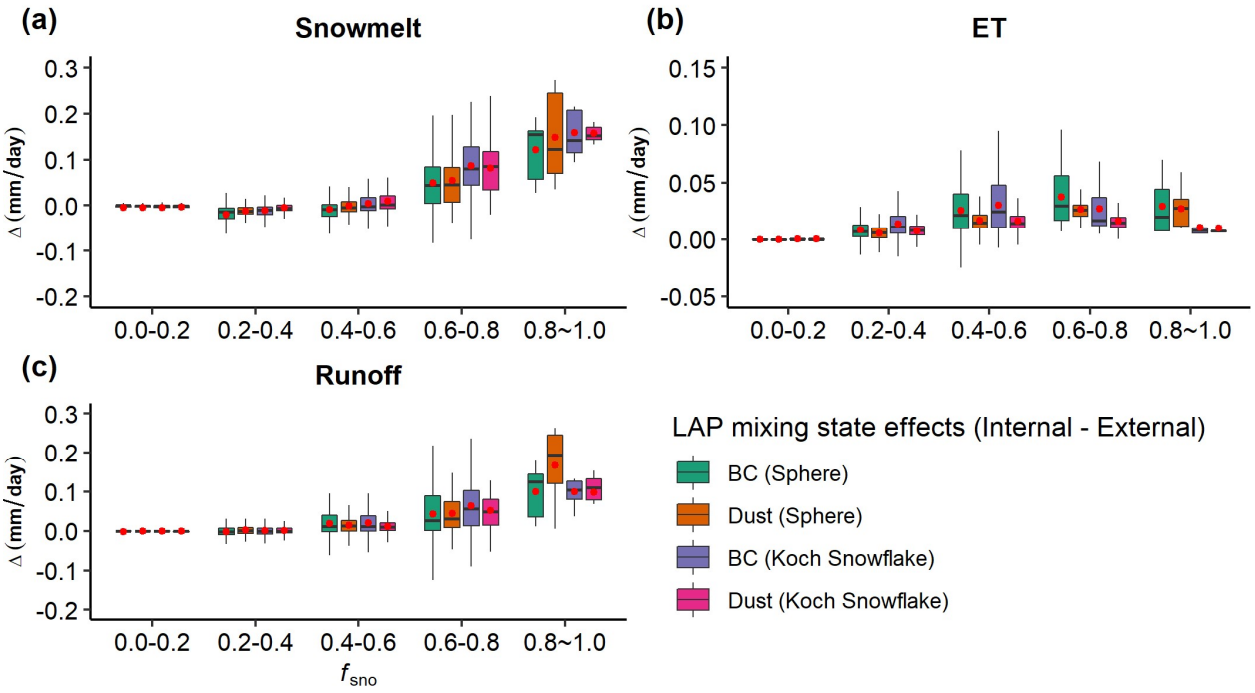

Figure S13: Same as Figure S9, except for hydrological terms: (a) snowmelt, (b) ET, and (c) runoff.

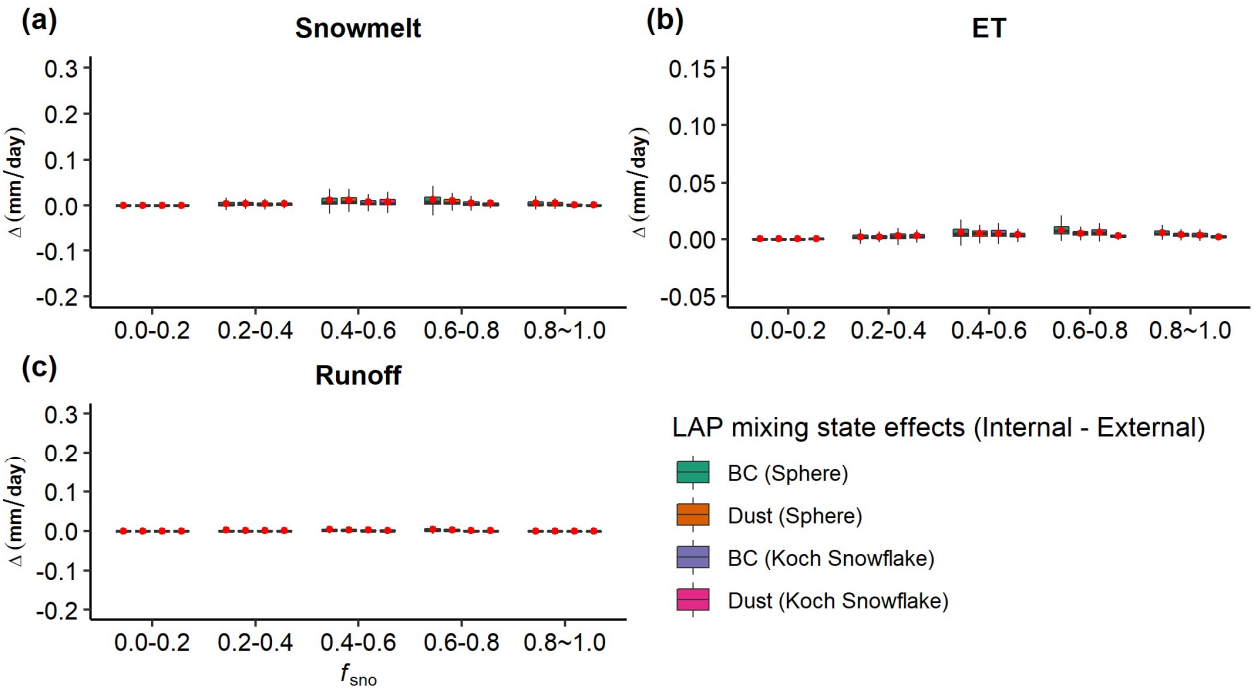

Figure S14: Same as Figure S10, except for hydrological terms: (a) snowmelt, (b) ET, and (c) runoff.

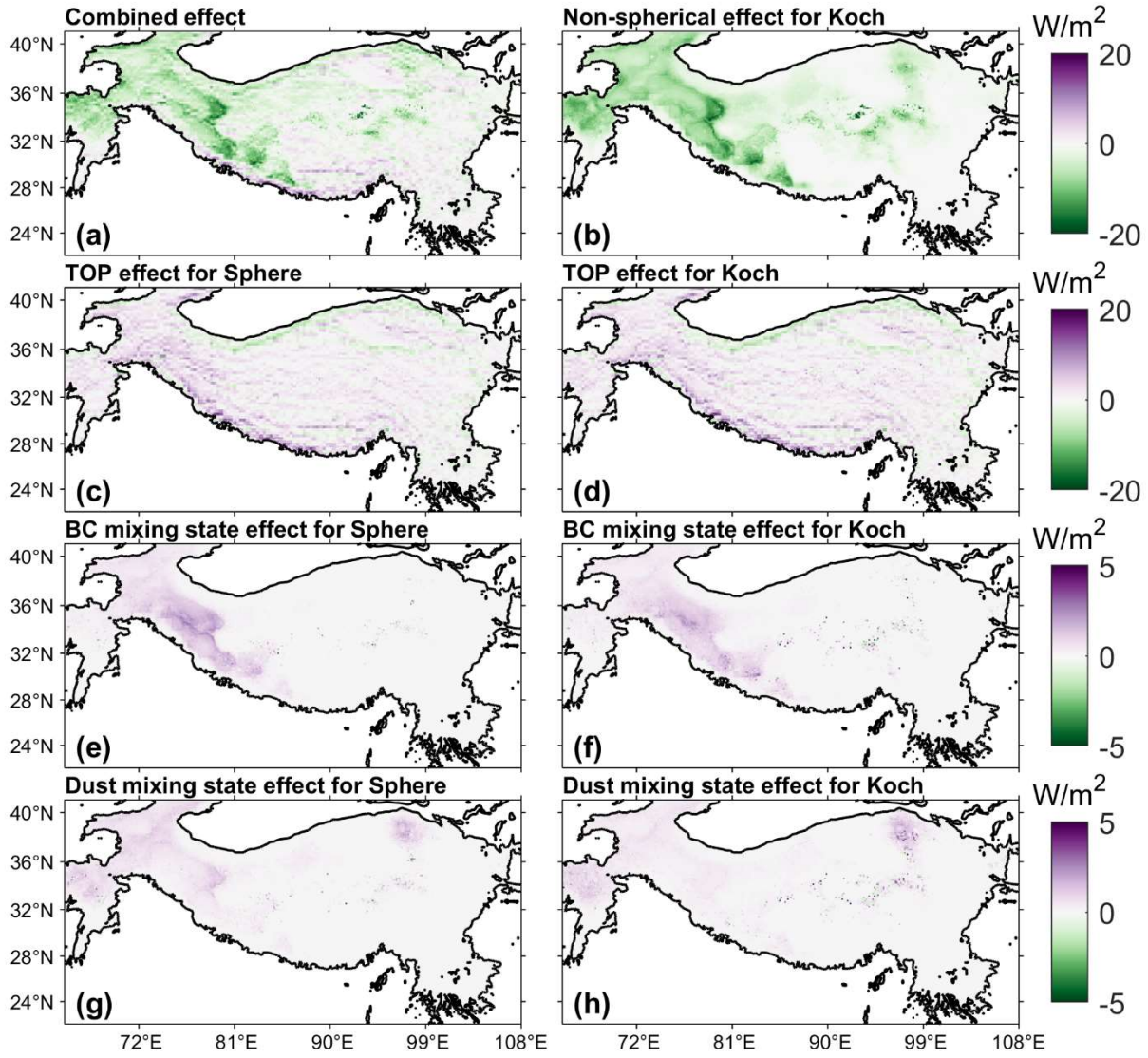

Figure S15: Spatial distributions of the change of net solar radiation contributed by different influencing factors and their combined effects in winter, which are derived based on Table 2.

Table S1. Statistics of RF values induced by different LAPs in winter and spring in the control simulations.

Aerosol type	Winter maximum	mean	Spring maximum	mean
All LAPs	6.4	0.7	21.9	1.3
BC	4.7	0.4	9.2	0.5
Dust	3.2	0.3	10.2	0.6

References

Bair, E., Stillinger, T., Rittger, K., and Skiles, M.: COVID-19 lockdowns show reduced pollution on snow and ice in the Indus River Basin, Proceedings of the National Academy of Sciences, 118, e2101174118, 2021.